ESI

X-ray characterisation

Laboratory XPD

BTS20 and BTS70 materials were pre-characterised using laboratory XPD to probe phase purity and sample equivalence. The figures S1-3 below show the diffraction data collected for the vacuum dried (VD), hydrated (H) and hydrated with D_2O (D) samples. No obvious secondary phases are present.

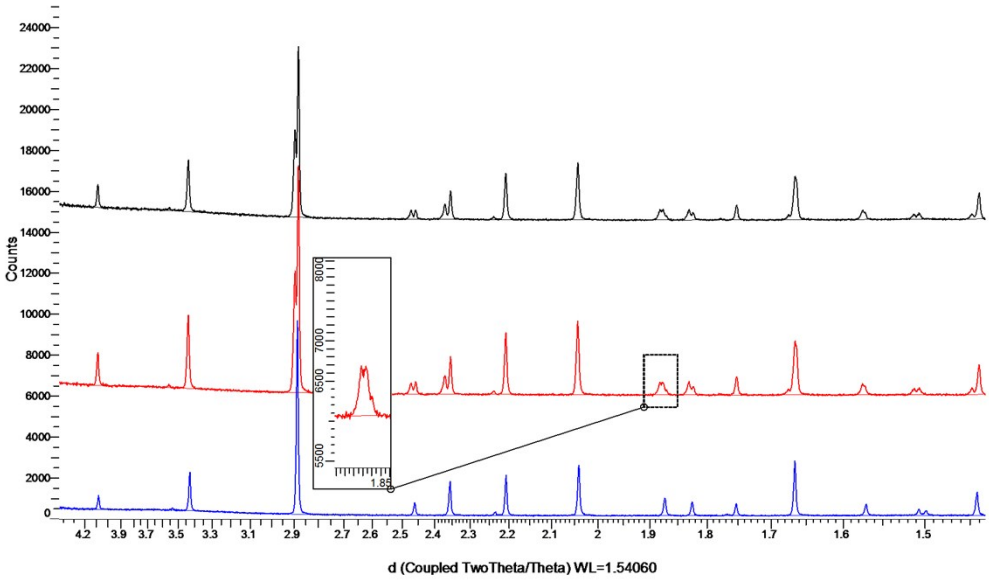

Figure S1 Laboratory XPD data for BTS20VD (blue), BTS20H (red) and BTS20D (black) showing the peak splitting that occurred upon hydration.

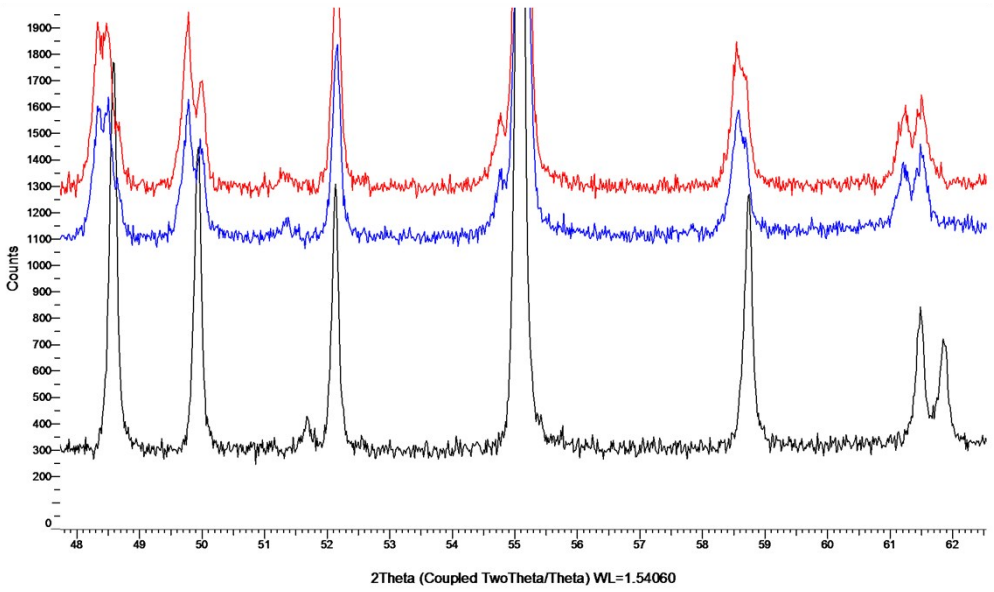

Figure S2 Expanded region of the laboratory XPD data showing the equivalent lattice parameters for BTS20H (red) and BTS20D (blue) samples compared with the smaller lattice parameter of the host materials BTS20VD (black).

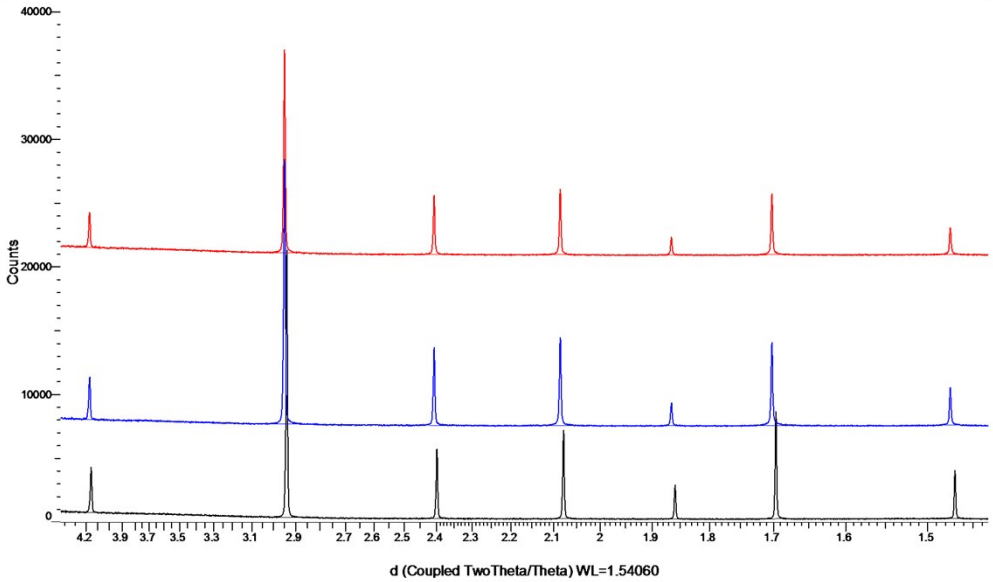

Figure S3 Laboratory XPD stack plot data for BTS70VD (black), BTS70H (blue) and BTS70D (red) illustrating the lattice parameter expansion upon hydration. No secondary phases were observed in the XPD data and the lattice parameters of the BTS70H and BTS70D samples are equivalent.

Synchrotron XPD

SXPD was used to evaluate the presence of minor secondary phases and also to probe whether any subtle symmetry reduction occurred in either the host or hydrated materials through the use of high-resolution data from ID22. Figures S4-S6 show data for BTS20 samples over the Q-range 1.2-7.5 $Å^{-1}$. Lattice parameters and volumes of BTS20H and BTS20D were equivalent when freely refined to within 0.01% for individual lattice parameters and 0.0003% for volume. Therefore, equivalence of hydration level in BTS20H and BTS20D could be assumed for modelling the NPD data. Figures S7-9 show data for BTS70 samples over a Q-range of 1.2-6.2 $Å^{-1}$ as peak intensity was found to rapidly fall off with increased Q. Lattice parameters and volumes of BTS70H and BTS70D were equivalent when freely refined to within the standard error of the refined variables (5^{th} decimal place). Therefore, equivalence of hydration level in BTS70H and BTS70D could be assumed for analysis of the NPD data. Very weak peaks indicative of $BaSc_2O_4$ were observed between Q-values of 2.2 and 2.25 $Å^{-1}$ when the data were highly magnified. These peaks are not easily visible in the Figures S7-9, illustrating the very low phase fraction. The oxygen content refined in the model presented in figure S7 is 0.865(10) using the NPD model to set the metal SOFs. None of the BTS70 samples show significant diffuse scattering in the SXPD data; scandium and titanium are equivalent in their number of electrons and the dominant scattering contribution is from the barium. Therefore the presence of a significant diffuse scattering component in the NPD data is indicative of local ordering of the lighter elements. Figure S10 shows the region around 2.6 $Å^{-1}$ for the three BTS70 samples highlighting the partial hydration for the SXPD sample, which is inconsistent with the TGA and NPD data, which show no hydration of the bulk BTS70VD sample. The broader peaks can be indexed with a lattice parameter intermediate between the host materials and the fully hydrated BTS70H sample. This supports the conclusion that the secondary phase in the SXPD was a result of an incompletely sealed capillary allowing hydration during transport to and measurement at the synchrotron source.

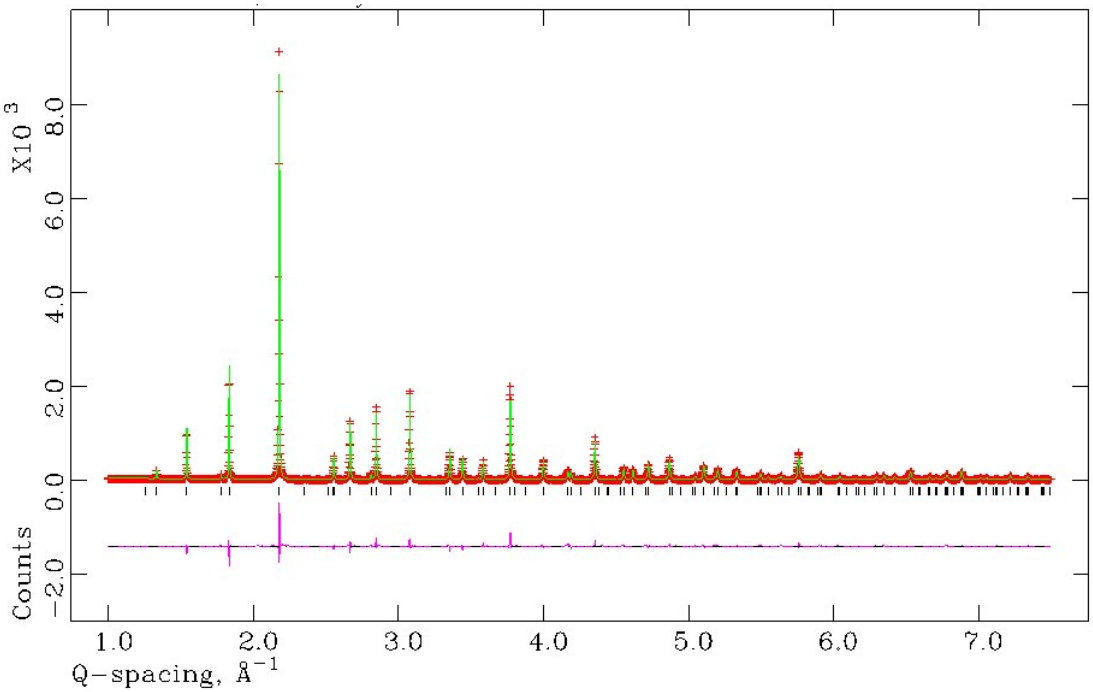

Figure S4 SXPD Rietveld fit to the BTS20VD sample. The observed data are red crosses, the fitted data the solid green line and the difference the magenta solid line.

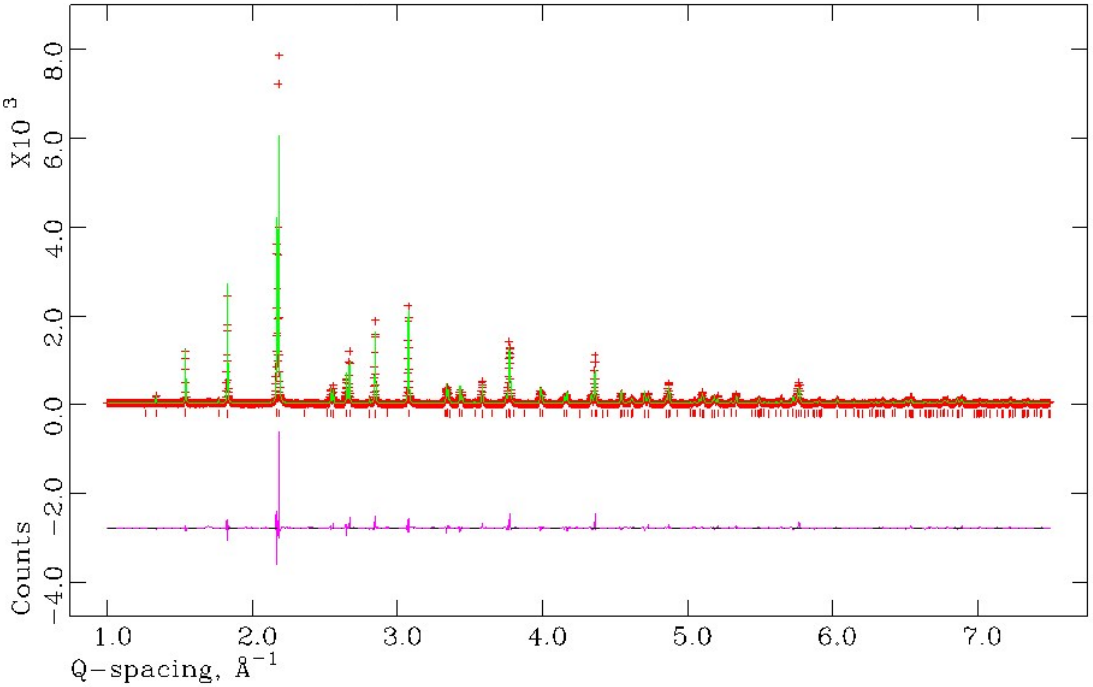

Figure S5 SXPD Rietveld fit to the BTS20H sample. The observed data are red crosses, the fitted data the solid green line and the difference the magenta solid line.

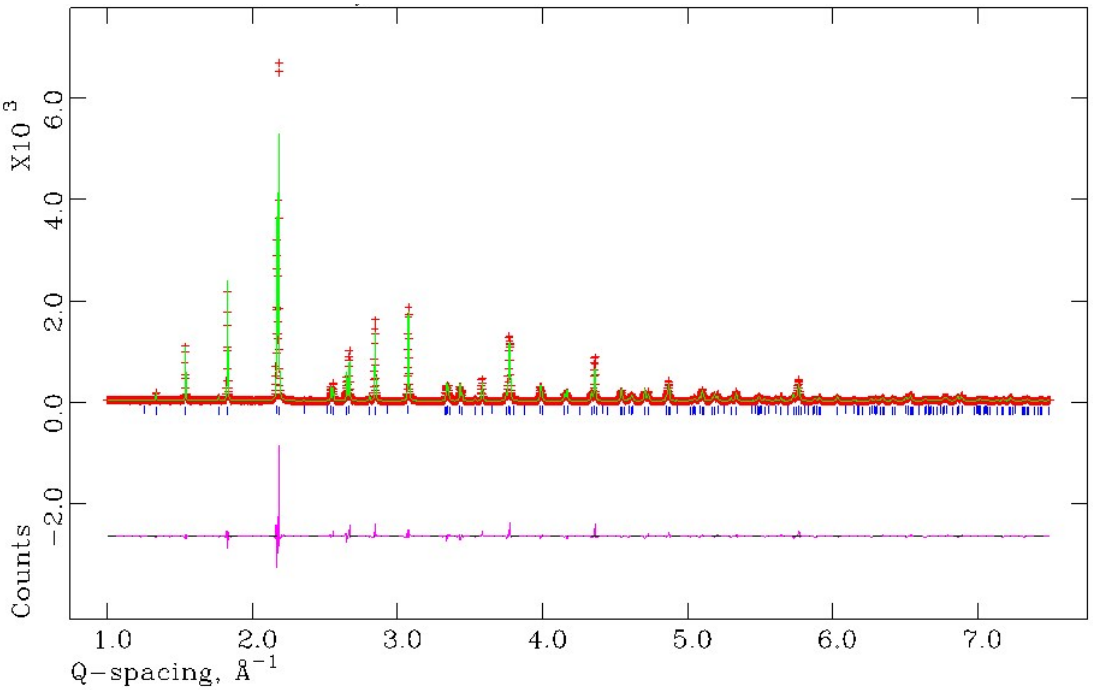

Figure S6 SXPD Rietveld fit to the BTS20D sample. The observed data are red crosses, the fitted data the solid green line and the difference the magenta solid line.

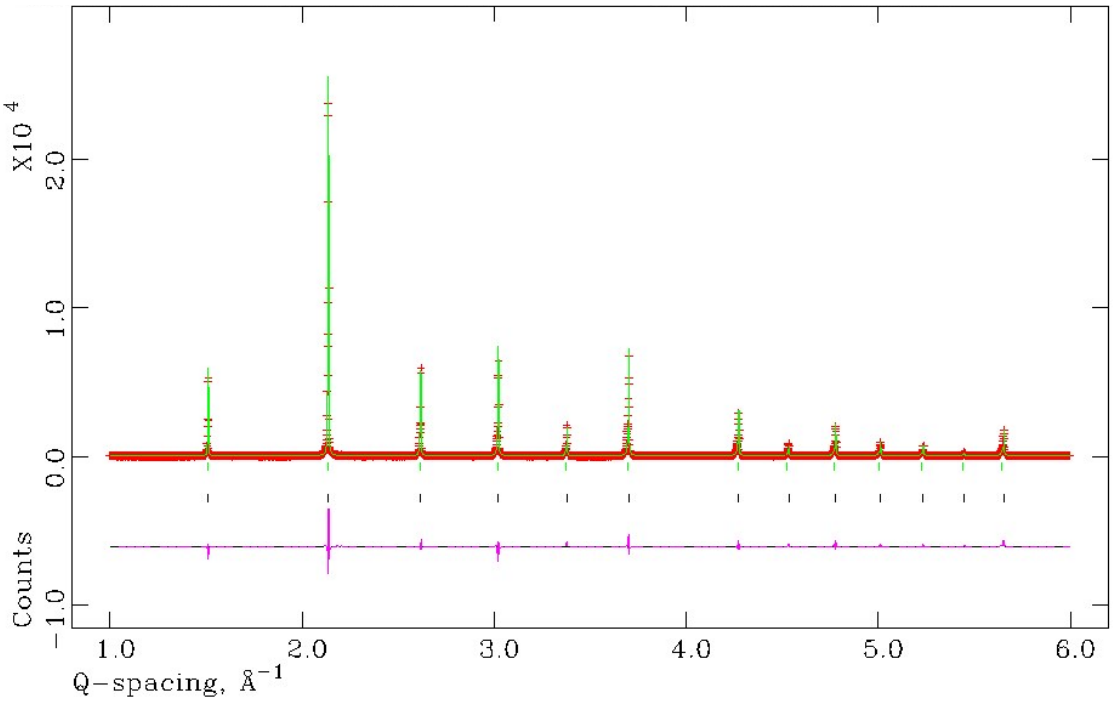

Figure S7 SXPD Rietveld fit to the BTS70VD sample. The observed data are red crosses, the fitted data the solid green line and the difference the magenta solid line.

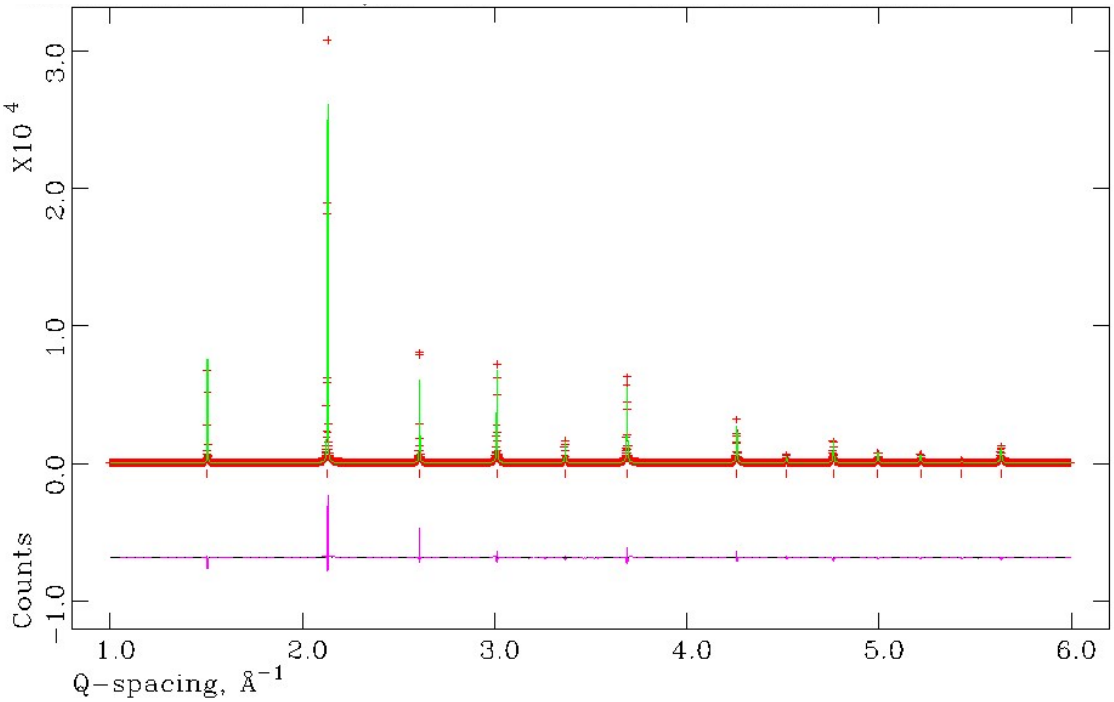

Figure S8 SXPD Rietveld fit to the BTS70H sample. The observed data are red crosses, the fitted data the solid green line and the difference the magenta solid line.

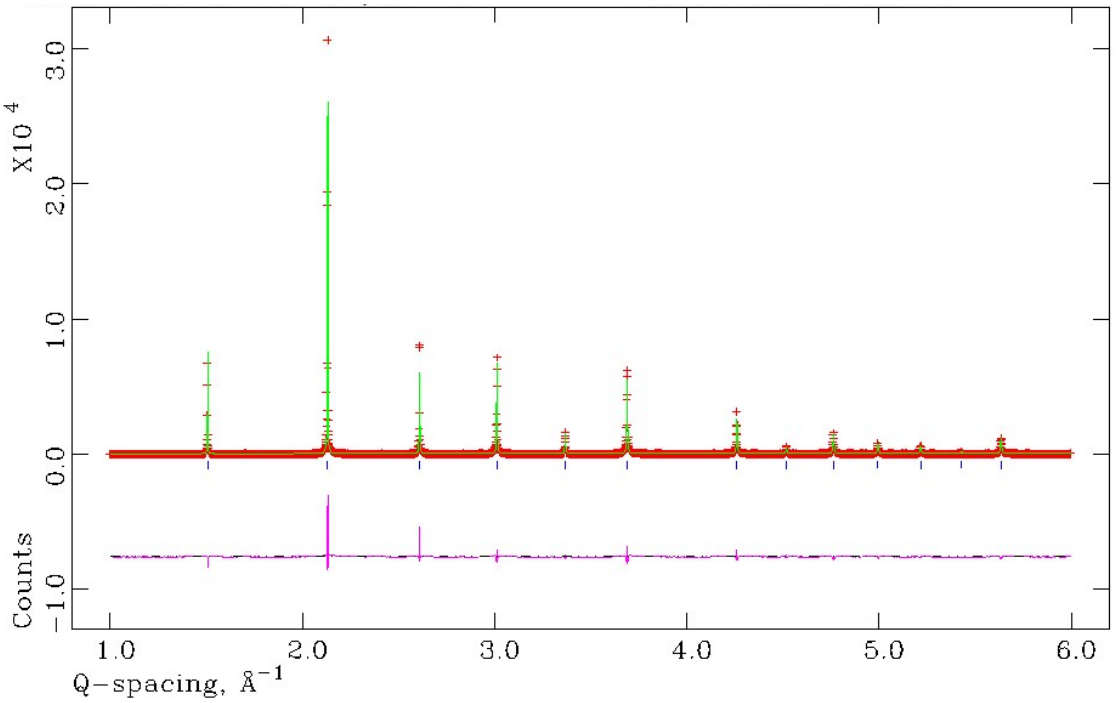

Figure S9 SXPD Rietveld fit to the BTS70D sample. The observed data are red crosses, the fitted data the solid green line and the difference the magenta solid line.

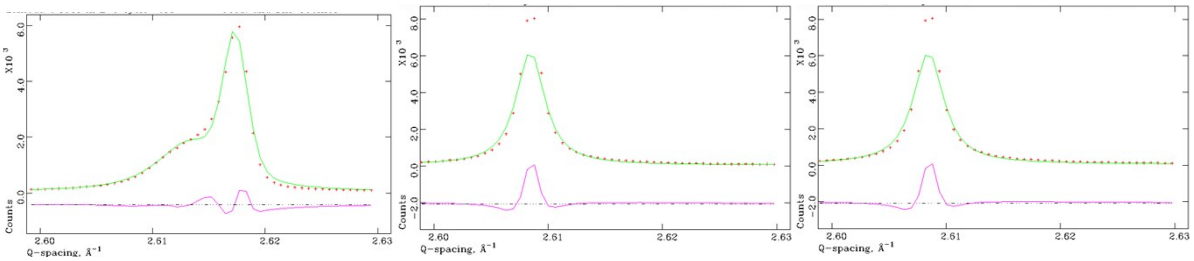

Figure S10 Expanded region from 2.6-2.63 $Å^{-1}$ from Figures S7-9 for (left) BTS70VD, (middle) BTS20H and (right) BTS20D showing the partial hydration of the BTS70VD sample. The broad peak (left) is intermediate between the fully hydrated phase (middle and right) and the host, vacuum dried phase (left). Both BTS20H and BTS20D (middle and right) show complete hydration and sample equivalence through identical lattice parameter expansion can be clearly seen.

TGA

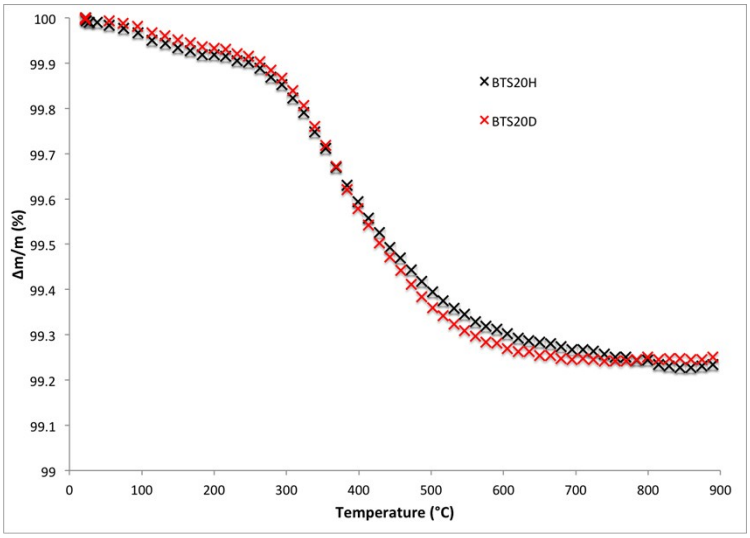

Figure S11 TGA plots for BTS20H (Black) and BTS20D (red) over the temperature range RT-900C.

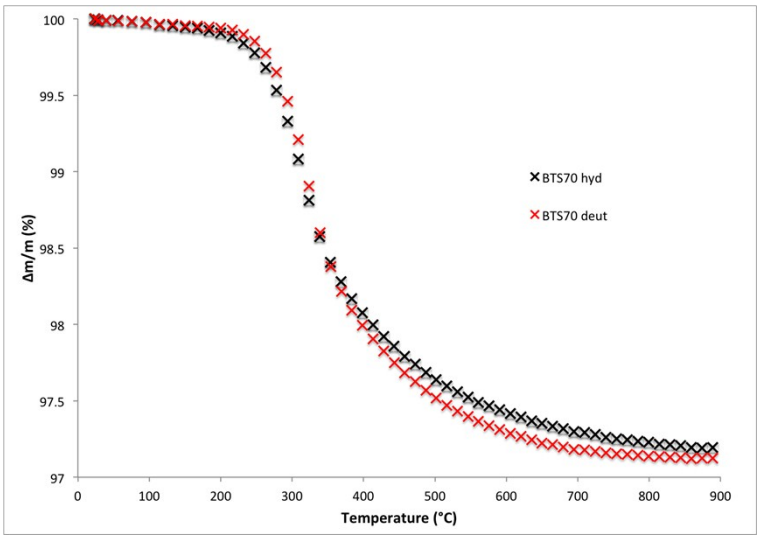

Figure S12 TGA plots for BTS70H (black) and BTS70D (red) over the temperature range RT-900C.

Table S1 Calculations of mass losses expected from TGA RT-900 °C for ideal and refined model stoichiometry

Sample	Stoichiometry	RMM	Mass loss on heating	%age mass loss on heating (2dp)
Ideal materials				
BTS20VD	$BaSc_{0.2}Ti_{0.8}O_{2.9}$	231.010042	0	0
BTS20H	$BaSc_{0.2}Ti_{0.8}O_{2.9}(H_2O)_{0.1}$	232.81157	1.801528	0.77
BTS20D	$BaSc_{0.2}Ti_{0.8}O_{2.9}(D_2O)_{0.1}$	233.0128024	2.0027604	0.86
BTS70VD	$BaSc_{0.7}Ti_{0.3}O_{2.65}$	225.554647	0	0
BTS70H	$BaSc_{0.7}Ti_{0.3}O_{2.65}(H_2O)_{0.35}$	231.859995	6.305348	2.72
BTS70D	$BaSc_{0.7}Ti_{0.3}O_{2.65}(D_2O)_{0.35}$	232.5643084	7.0096614	3.01
Refined stoichiometry				
BTS20VD	$BaSc_{0.2}Ti_{0.8}O_{2.899}$	230.9940426	0	0
BTS20H	$BaSc_{0.2}Ti_{0.8}O_{2.902}(H_2O)_{0.098}$	232.8075382	1.81349564	0.78
BTS20D	N/A	N/A	N/A	-
BTS70VD	$BaSc_{0.661}Ti_{0.339}O_{2.65}$	225.6681795	0	0
BTS70H	$BaSc_{0.661}Ti_{0.339}O_3H_{0.72}$	231.9936863	6.32550681	2.73
BTS70D	N/A	N/A	N/A	-

Neutron characterisation

RT v 5K

The manuscript compares models based on the RT datasets for both BTS20 and BTS70. The reason for this is the observation of several weak peaks in the BTS70 data at low temperature that were not visible at room temperature (Figure S13). A phase transition indicative of oxygen vacancy ordering in the VD sample and proton ordering in the H and D substituted samples could not be ruled out. As the peaks were not present in the RT data (the only extra peaks are from the vanadium can and traces of $BaSc_2O_4$) model comparison used the RT data. Further variable temperature *in situ* NPD is required to follow the evolution of the structure as a function of temperature to investigate the origin of the weak peaks. The Tables S2-3 compare the refined models at 5K and RT assuming no phase transitions for the BTS20 and BTS70 compositions respectively. No major differences are observed and, therefore, we believe the room temperature models presented are robust.

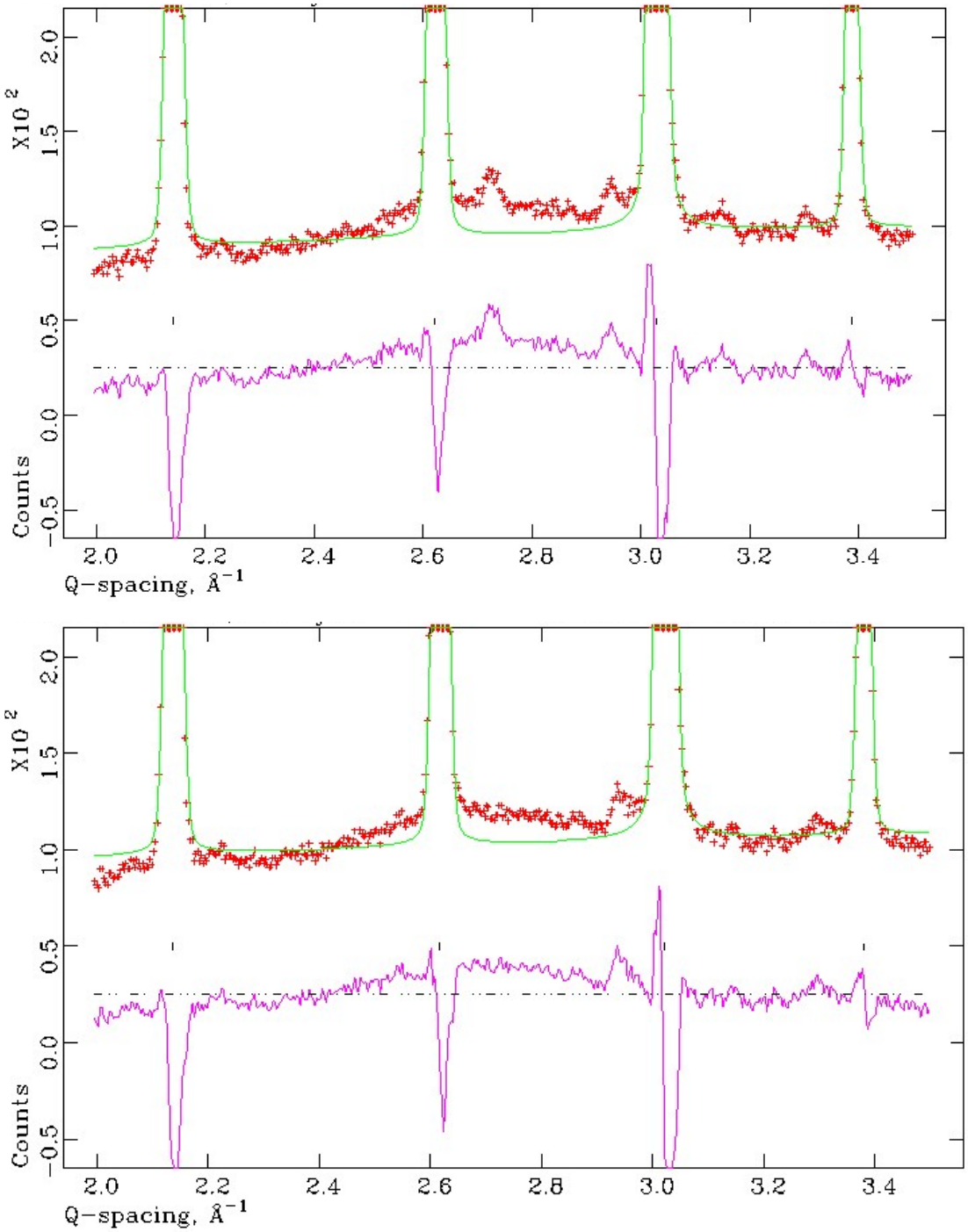

Figure S13 Expanded region of the Rietveld refinement fits at 5K (upper) and RT (lower) of BTS70VD showing the presence of weak reflections at 2.73 $Å^{-1}$ and 3.14 $Å^{-1}$ in the 5K data.

Table S2 Comparison of the refined models for BTS20VD and BTS20H at RT and 5K. The extracted compositions and O1-H bond length are also given.

BTS20	RT		5K	
	VD	H	VD	H
a (Å)	5.7699(1)	5.7624(1)	5.7583(1)	5.7506(1)
c (Å)	14.1408(3)	14.2242(3)	14.1133(3)	14.1991(4)
Volume (Å^3)	407.70(1)	409.04(2)	405.27(1)	406.64(2)
Ba(1) *2b* (0, 0, 1/4)				
U_{iso} (Å^2)	0.0047(7)	0.0047(7)	0.0009(8)	0.0009(8)
Ba(2) *4f* (1/3, 2/3, *z*)	0.09662(14)	0.09662(14)	0.09645(16)	0.09645(16)
U_{iso} (Å^2)	0.0075(6)	0.0075(6)	0.0033(6)	0.0033(6)
Sc / Ti *2a* (0, 0, 0)				
Occ. Factor	0.526(3) / 0.474(3)	0.526(3) / 0.474(3)	0.527(4) / 0.473(4)	0.527(4) / 0.473(4)
U_{iso} (Å^2)	0.0046(8)	0.0046(8)	0.0045(9)	0.0045(9)
Ti / Sc *4f* (1/3, 2/3, *z*)	0.84684(23)	0.84684(23)	0.84617(27)	0.84617(27)
Occ. Factor	0.963(2) / 0.037(2)	0.963(2) / 0.037(2)	0.959(2) / 0.041(2)	0.959(2) / 0.041(2)
U_{iso} (Å^2)	0.0045	0.0045	0.0045	0.0045
O(1) *6h* (*x*, *y*, 1/4)	0.51626(21)	0.51626(21)	0.51600(23)	0.51600(23)
	0.03242(43)	0.03242(43)	0.03190(47)	0.03190(47)
Occ. Factor	0.899(5)	1.0	0.900(6)	1.0
U_{iso} (Å^2)	0.0145(5)	0.0145(5)	0.0112(5)	0.0112(5)
O(2) *12k* (*x*, *y*, *z*)	0.83126(13)	0.83126(13)	0.83126(15)	0.83126(15)
	0.66244(27)	0.66244(27)	0.66242(29)	0.66242(29)
	0.08241(6)	0.08241(6)	0.08262(7)	0.08262(7)
U_{iso} (Å^2)	0.0066(2)	0.0066(2)	0.0040(3)	0.0040(3)
H / D *12j* (x, y, 1/4)		0.354(5)		0.357(5)
		0.496(5)		0.490(5)
Occ. Factor		0.098(6)		0.110(7)
U_{iso} (Å^2)		0.025		0.020
R_{wp} (%)	5.88	4.79	6.72	5.79
$R_{F\hat{}2}$ *(%)*	4.33	6.75	6.19	8.58
Refined Composition				
Ba	1.0	1.0	1.0	1.0
Sc	0.200(6)	0.200(6)	0.203(6)	0.203(6)
Ti	0.800(6)	0.800(6)	0.797(6)	0.797(6)
O	2.899(5)	3.0	2.900(6)	3.0
H	0	0.196(10)	0	0.220(10)
O1-H bond length		0.970(27)		0.934(28)

Table S3 Comparison of the refined models for BTS70VD and BTS70H at RT and 5K. The extracted compositions and O-H bond length are also given.

BTS70	*RT*		*5K*	
	VD	*H*	*VD*	*H*
a (Å)	4.15663(3)	4.17150(8)	4.14779(3)	4.16284(8)
Volume (Å^3)	71.816(1)	72.590(3)	71.359(1)	72.139(3)
Ba *1b* (1/2, 1/2, 1/2)				
$U_{11} = U_{22} = U_{33}$ (Å^2)	0.0200(4)	0.0200(4)	0.0178(4)	0.0178(4)
$U_{12} = U_{13} = U_{23}$ (Å^2)	0	0	0	0
Sc / Ti *1a* (0, 0, 0)				
Occ. factor	0.661(3) / 0.339(3)	0.661(3) / 0.339(3)	0.658(3) / 0.342(3)	0.658(3) / 0.342(3)
$U_{11} = U_{22} = U_{33}$ (Å^2)	0.0097(4)	0.0097(4)	0.0098(4)	0.0098(4)
$U_{12} = U_{13} = U_{23}$ (Å^2)	0	0	0	0
O *3d* (1/2, 0, 0)				
Occ. factor	0.883	1.0	0.883	1.0
U_{11} (Å^2)	0.0172(8)	0.0172(8)	0.0174(8)	0.0174(8)
$U_{22} = U_{33}$ (Å^2)	0.0291(5)	0.0291(5)	0.0263(5)	0.0263(5)
$U_{12} = U_{13} = U_{23}$ (Å^2)	0	0	0	0
H / D *24k* (x, y, 0)		0.241(8) 0.399(6)		0.0232(8) 0.0398(6)
Occ. factor		0.03		0.03
U_{iso} (Å^2)		0.025		0.020
R_{wp} (%)	7.46	6.32	8.09	6.58
R_{F^2} (%)	15.50	15.43	10.21	15.72
Refined composition				
Ba	1.0	1.0	1.0	1.0
Sc	0.661(3)	0.661(3)	0.658(3)	0.658(3)
Ti	0.339(3)	0.339(3)	0.342(3)	0.342(3)
O	2.65	3.0	2.65	3.0
H	0	0.72	0	0.72
O-H bond length		1.089(33)		1.054(33)